Research Article

Growth of glassy carbon thin films and its pH sensor applications

Ryosuke Shinzawa[1] · Ayaka Otsuka[2] · Atsushi Nakamura[1,2]

Abstract

Glassy carbon (GC) thin film was successfully deposited via thermal pyrolysis of ethanol vapor by means of chemical vapor deposition at 1000 °C without any catalysis. The Raman spectra of the grown GC film showed typical peaks of D1, G, and 2D1 including derivative peaks of D2 band and a combinational peak of D1 + G that indicates the film is glassy carbon. XPS analysis of the C 1s core showed the deposited films have carbon atoms consisting of an almost sp^2 binding structure. A picture of the cross-sectional transmission electron microscope showed the stacking layers of a disordered carbon have a turbostratic layer with a few nanometers graphitic domain, about 13 nm estimated by Raman spectra. Two types of pH sensor were fabricated. One is a GC based field-effect transistor with a top gate of a solution (GC-FET), and the other is a GC extended gate electrode connected to commercial Si FET (GC-EGFET). The average pH sensitivity of GC-FET and GC-EGFET is 21.5 mV/pH and 26.5 mV/pH, respectively, which are comparable for graphene-based solution gating pH sensors that have appeared in the recent literature.

Keywords Glassy carbon · Chemical vapor deposition · Solution gate field-effect transistor · Extended gate field-effect transistor · pH sensor

1 Introduction

Glassy carbon (GC) is a technologically important material and the GC electrodes have been widely used due to their excellent properties including strong corrosion resistance, chemical inertness, thermal stability and a structure impermeable to both gases and liquids, wide electrochemical potential window, electrocatalytic activity for redox reactions, good electrical conductivity, good biocompatibility, and low fabrication costs [1–4]. Therefore, not only the GC, but also various carbon allotropes like graphite, graphene, carbon nanotubes, and pyrolytic carbon has been utilized for various applications including electro-analysis, electro-catalysis, energy conversion, energy storage, and sensors [5–14].

Despite numerous reports in utilizing GC electrodes including the surface absorption of molecules to emphasize sensing properties, a synthesis and/or growth study on the planer two-dimensional structure of GC has not yet been reported. The microstructure of GC is a network of turbostratic curved graphitic carbon planes with graphitic sp^2 hybridization of C bonds, like highly disorder graphite without dangling bonds [3]. Currently, GCs have made from an organic polymer resin [1–3]. One example is synthesized by a decomposition of a cross-linked polymer like a resin of phenol-hexamine [2, 3]. It can be synthesized by carbonization of alcohol precursors. If we could prepare the GC into a planer film, it can be substituted for other carbon allotropes like graphite, carbon nanotubes, and graphene. Indeed, several approaches to obtain thin

carbon films have been investigated such as a pyrolysis of photoresists [12, 15–17] and a screen-printing ink [18, 19]. These techniques have an advantage of the simple process, highly reproducible and facile desirable patterns. However, pyrolysis carbon shows a structure with a microstructure composed of both graphitic and amorphous, the electrical resistivity is still high for the sensing electrodes [12]. The latter technique has several issues to overcome such as uniformity of dispersed ink, removing the dispersant, and a cost of fabrication ink [19]. A promising approach to obtain thin GC film is through the pyrolysis of alcohol vapor by means of chemical vapor deposition directly on substrates without any catalysts. GC processed using CVD exhibits several advantages, including good electrical and chemical properties, a large area deposition resulting in low cost fabrication. Moreover, this technique has advantages of the large scales, the simple process, and a low cost compared with preceding graphene and SWCNTs. A large-scale GC film across an entire substrate contrasts with the conventional micromechanical exfoliated graphene which graphene is prepared in the form of small flakes [20]. Furthermore, it enables to avoid the transfer process in contrast to CVD graphene grown on metal catalyst substrates [21] and a solution process of dispersed SWCNTs [22]. The transfer process causes an introduction of defects, impurities, and cracks into graphene even though high-quality and highly uniform graphene can be obtained using CVD. The SWCNT technique has several issues to overcome such as uniformity of dispersed solution, removing the dispersant, and a cost of purifying solutions. As-synthesized SWCNTs are often contaminated with amorphous carbon and residual catalyst particles, which have been limited by both the high cost of the nanotubes and difficulties associated with the processing of the as-produced materials [22–25]. As described above, therefore, an alternative material of allotrope is required such as GCs for industrial production.

In this study, we have an attempt to synthesize GC film directly on substrates by CVD using ethanol. Grown GC films were evaluated by Raman spectroscopy, X-ray photoelectron spectroscopy, and transmission electron microscope for the crystallinity of film state GCs. Furthermore, we demonstrate a solution-gated GC film field-effect transistor (FET) and an extended gate FET using the same device structure to evaluate the electrical characteristics for the GC film. The observed sensitivity of 20 mV/pH and 28 mV/pH respectively is in good agreement with results obtained on graphene surfaces. Our experiments indicate the potential of this new glassy carbon film-based device in pH sensing applications.

2 Experimental section

2.1 Synthesis of the glassy carbon films

Glassy carbon films were deposited on 10–15 mm squares thermally oxidation SiO_2 on p-type Si wafers and both sides polished r-plane (01–12) sapphire substrates. Prior to growth, the substrates were cleaned followed by acetone and ethanol, H_2O_2/H_2SO_4 solution for 15 min at 60 °C and then rinsed with water. Glassy carbon films were grown with a home-built chemical vapor deposition (CVD) system using ethanol vapor as the carbon feed stock and ultrahigh purity argon (99.999% purity) as the carrier gas as showed in Figure S1 in supplementary materials. The substrates were placed into the tubular furnace and the reaction chamber was evacuated to 0.01 Torr. Then 180 sccm Ar was introduced into the CVD chamber with a pressure of 10 Torr and the temperature was raised to 1000 °C. After stabilization, we introduced 1 sccm ethanol into the system while keeping the ethanol flow for 10, 30, and 60 min, during which glassy carbon growth occurred. After that, the ethanol flow was turned off, and the substrate was naturally cool down to room temperature.

2.2 Electrolyte preparation

The pH solutions of a phthalate buffer solution at pH 4.01, a phosphate buffer solution at pH 6.86 and a borate buffer solution at pH 9.18, and 0.1 mol/L of sodium hydroxide solution, and sodium chloride were purchased from Fujifilm Wako pure Chemical Corporation. A pH 12.0 of the solutions was adjusted by adding aliquots of sodium hydroxide (NaOH) solution. The pH of the solutions was adjusted to a total ionic strength of 10 mM by adding NaCl and distilled water.

2.3 Sensor device fabrications

The configuration of the GC FET pH sensor is illustrated in Fig. 1. The sensor is composed of source and drain electrodes incorporating with synthesized GC film serving as a conductive channel of the FET. In this study, we examined two types of pH sensor. One is solution top gate FET structure (GC-FET) and the other type is extended gate FET structure (GC-EGFET). Briefly, for the GC-FET, the fabrication process of the FET device starts with the preparation of a chip with two electrodes, i.e. source and drain as showed in Fig. 1a, b. Figure 1a shows the photograph of the sensor chip and Fig. 1b illustrates the schematic configuration of the sensor top view and the cross-sectional view. The GC film sample was stuck on
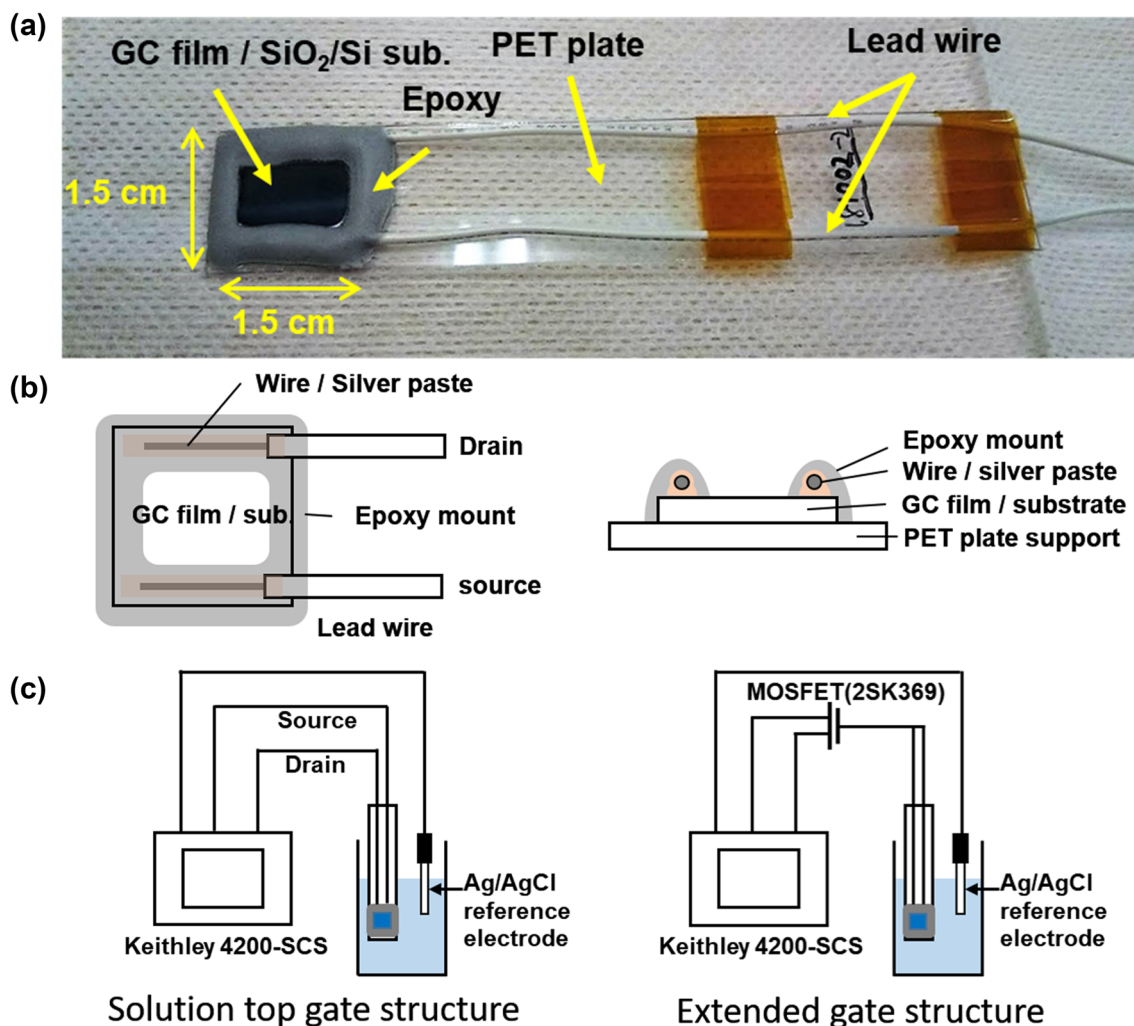
Fig. 1 Schematic configuration of the sensing performance measurement system of solution gated CG FET and extended gate FET pH sensors. **a** The photograph of the sensor chip, **b** schematic illustrations of the structure of the sensor chip for the top view and the cross-sectional view, **c** the measurement system for the solution top gate structure and the extended gate structure

a 20 mm × 150 mm × 0.5 mm-thick cut PET plate with a double-sided carbon tape. 0.5 mm-diameter of the lead wires were attached to a silver paste on the side of the GC film surface to form the source and drain electrodes. Finally, the electrodes area was encapsulated by an epoxy resin to protect the electrodes and the connection of lead wires from the electrolyte. The source and drain electrodes are with a gap distance of about 1 cm. The sensing area of the sensor is designed as 1 cm in width and 1 cm in length (i.e. 1 cm^2). For the extended gate FET structure (GC-EGFET), EGFET was separate into two parts. One was the sensing structure containing the sensitive membrane, which is basically the same setup of the GC-FET sensor chip, and the other was the MOSFET structure. The sensitive membrane of the GC surface is connected by short-circuiting between the source and the drain by means of attaching to the gate electrode of the MOSFET as showed

on the right side of Fig. 1c. The sensing structure and the reference electrode were dipped into the buffer solution and connected to the gate of MOSFET. Our MOSFET is a commercial device 2SK369.

2.4 Sample characterization

Raman spectra were carried out by micro-Raman analysis (NRS-7100, JASCO) with an excitation laser wavelength of 532 nm. Transmittance spectra were recorded using a JASCO UV–Visible Spectrophotometer V-670. Morphological features of the synthesized glassy carbon films were examined using field emission scanning electron microscope (FE-SEM) (JSM-7001F, JEOL), atomic force microscope (AFM) (SPI-3800, SII), and transmission electron microscope (TEM) (JEM2100F, JEOL). The X-ray photoelectron spectroscopy (XPS) measurements have been

performed in a SHIMAZU ES-3400, equipped with an Mg Kα monochromatic X-ray source ($h\nu = 1253.6$ eV), and was investigated to analyze the elemental compositions of glassy carbon films on SiO_2/Si substrate and HOPG as a reference graphitic carbon structure. The sheet resistivity of the samples was carried out by the four-probe method using a four-probe cable (SR4-S, Astellatech, Inc. Japan) attached to a DC voltage and current source/monitor (R624A, Advantest, Japan). The electrical characteristics of the FET devices were measured by a Keithley 4200-SCS (Semiconductor Characterization System) with an Ag/AgCl reference electrode (BAS Inc., Japan) as the top gate electrode.

3 Results and discussion

3.1 Morphological characterization

Figure 2a–c show the FE-SEM images of glassy carbon film deposited for 10 min, 30 min, and 60 min, respectively.

Figure 2d–f show the AFM images of the samples (a–c), and the bottom part shows the scan profiles indicated in the AFM images, respectively. It can be seen the film consists of nanoparticle-like structures with a few tens of nm size, which closed packed together with increasing the growth time, resulting in forming a three-dimensional structure with a large surface area. RMS in the roughness of the film surface was increased from 1.9 nm for 10 min, 4.0 nm for 30 min to 7.8 nm for 60 min. Although the film deposited for 10 min and 30 min is essentially uniforms, the domains of the GC for 60 min are larger and the surface looks bumpier in the AFM images, but the FE-SEM images are looked smooth surface. It was difficult to ascertain the film thickness due to the high surface roughness. The deposited film thickness was roughly estimated in Supplementary materials.

Typical cross-sectional TEM micrographs of GC film grown on SiO_2/Si substrate at 1000 °C is shown in Fig. 3. The microstructure of the glassy carbon layer appears turbostratic graphitic layers as the disordered network, which is marked by arrows. It is noted the obscurity fragments
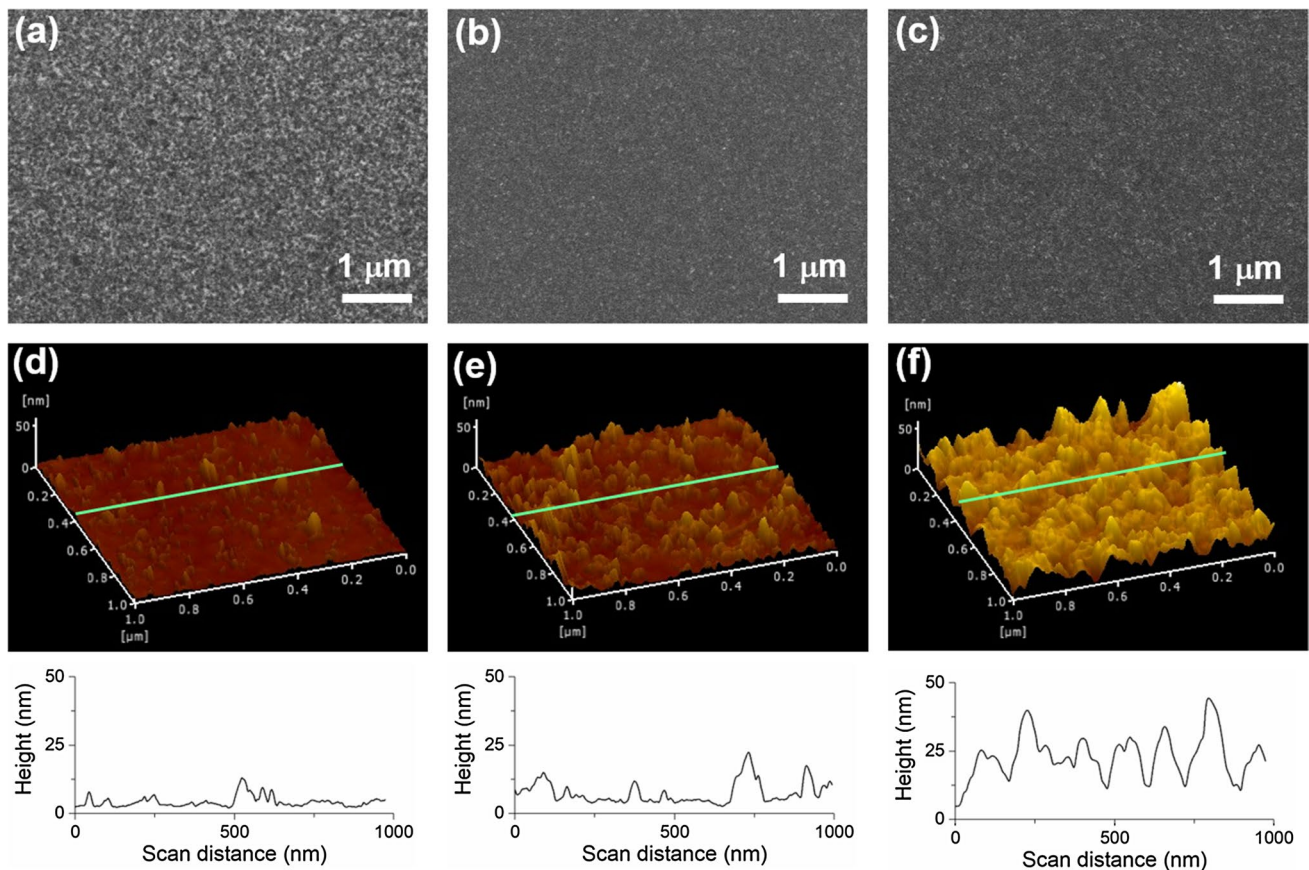

Fig. 2 FE-SEM images of glassy carbon films directly grown on SiO_2/Si substrate with different growth time; **a** for 10 min, **b** for 30 min, and **c** for 60 min, respectively. AFM images of the samples; **d** for 10 min of sample (**a**), **e** for 30 min of sample (**b**), and **f** for 60 min of sample (**c**), respectively. The bottom insets show scan profiles indicated in the AFM images respectively
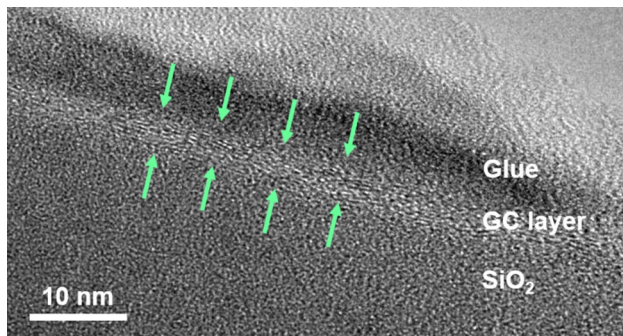
Fig. 3 High-resolution TEM image of GC film grown on SiO_2/Si substrate at 1000 °C
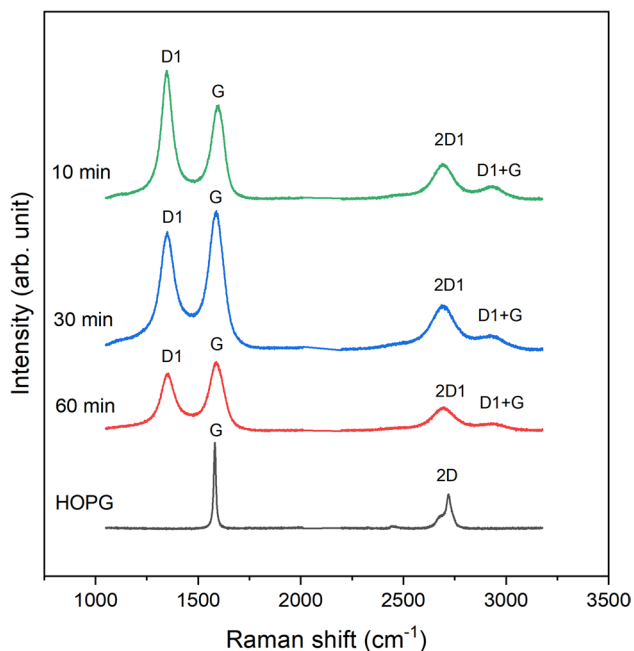

Fig. 4 Overview of the Raman spectra for GC films grown at 1000 °C for different growth time from the range of 10–60 min, and HOPG as a reference for graphite structure

of the glassy carbon layers may be weakly oriented to the substrate with small domains. The lateral domains of the carbon nanolattices appear 3–5 nm and exhibit lattice spacing of 0.3–0.5 nm. It is interesting that the microstructures of the GC film are comparable to the graphitizing carbon prepared by pyrolysis of anthracene at 1000 °C [3, 23–26].

3.2 Structural characterization

Figure 4 shows the Raman spectra for GC film grown at 1000 °C for different growth time and HOPG as a reference for the graphite structure. Similar spectra were obtained

from the glassy carbon prepared by annealing at 1500 °C in the literature [4, 27–31]. The first-order and the second-order Raman spectra were observed. The first-order Raman spectra of GC is shown dominantly two peaks, where are at around 1580 cm^{-1} (*G* peak) and at around 1350 cm^{-1} (*D* peak). The *G* peak is assigned to lattice vibration in the plane of the graphite-like nano-particles in the GC structure [31]. The *D* peak is the so-called disorder peak and is frequently seen in small crystallite size of graphitic materials. The *D* peak is negligibly small for the HOPG. Line decomposition of the raw spectrum of the first-order Raman spectrum into three bands is also presented in Supplementary Figure S4. There is a small peak at around 1615 cm^{-1} (*D'* peak) which located in a high-wave-number side of the *G* peak. Since the *D'* peak is often small, it is difficult to decompose from the combinational peak of *G* and *D'*, however, we can observe the broad and higher peak position of "*G* peak" compared with the *G* peak of graphite (HOPG). The second-order Raman spectra of GC is also dominated by two peaks, where are the overtones of the *D*1 peak at around 2710 cm^{-1} (2*D*1 peak) and the combined tone at around 2930 cm^{-1} (*D*1 + *G* peak) [31]. In the case of graphene, a single layer of graphite, the 2*D*1 peak appears a single sharp peak. When graphene layers increase numbers of layers in the stack, the 2*D*1 peak height decreases significantly. Finally, the 2*D* peak in bulk graphite consists of two components 2*D*1 and 2*D*2 [32]. For the glassy carbon, the intensity of the 2*D*1 peak decreases with an increase in the growth time. It is likely to be the effect of an increase in numbers of layers in the graphite-like domains, as can be seen in the transmittance spectra in Fig. S2. Moreover, low intensity of the 2*D*1 bands for 10 min glassy carbon may be explained by the small lateral size of the graphene-like domains and the high defect densities as a high I_D/I_G ratio [33].

3.3 Chemical characterization

Figure 5a depicts the XPS survey spectra for the GC film with different growth time and HOPG. The HOPG sample was peeled off the several layers from the surface by plastic tape to expose fresh plane. The spectra of GC film and HOPG exhibit the characteristic C1s peak at 284 eV [34]. The 10 min GC film also exhibits C 1s including Si 2p, Si 2s, and O 1s peaks. They are ascribed to the SiO_2/Si substrate. The C1s core level XPS spectrum (Fig. 5b) is dominated by a peak at 284 eV assigned to the sp^2 carbon framework and sp^3 hybridized state at 285 eV which located on the high binding energy side of the main peak line [34]. These spectral features in the GC film are almost like the HOPG, suggesting that the carbon of GC structure exhibit sp^2 formations. The decomposition of the sp^3 hybridized state can be assigned to carbon-hydrogen
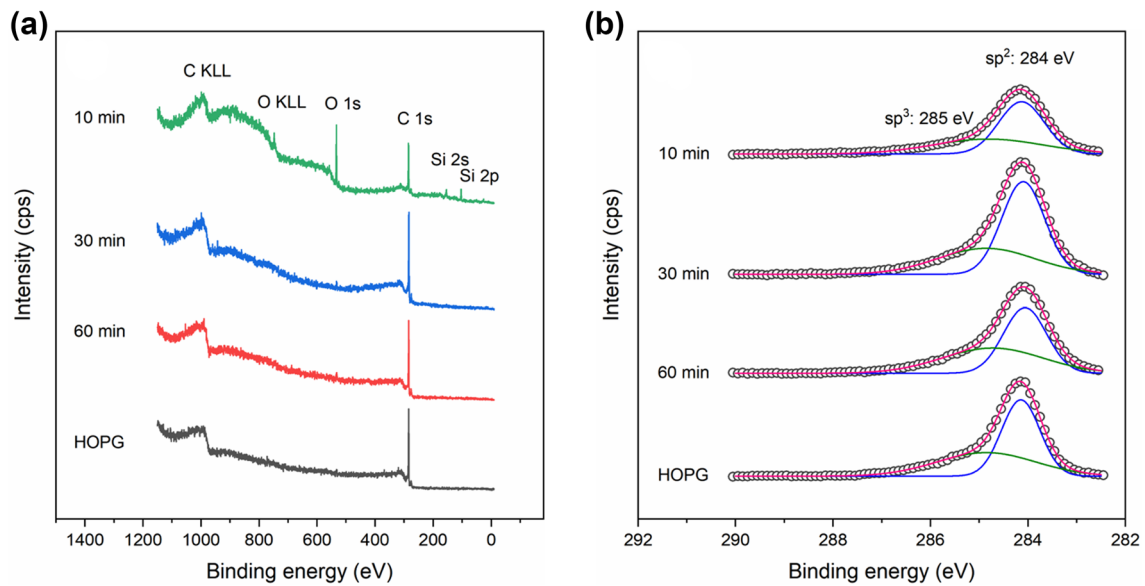
Fig. 5 XPS spectra of GC films with different growth time and HOPG as a comparison. **a** XPS survey spectra and **b** XPS C1s core level spectra for the GC films and HOPG

bonded groups that occur when the carbon atoms have a chemical environment experienced. The characterization of GC including XPS results suggest that although the GC film has a highly disordered structure, a rough surface (in other words of a high surface-volume ratio), the layered structure shows sp^2 carbon layers as well as bulk graphite, and we can utilize the film as an alternate for graphene, reduced graphene oxides (rGOs), and/or carbon nanotubes (CNTs).

3.4 Electrical characterization

Prior to fabrication of pH sensor devices, we tested a sheet resistance (Rs) of GC film using a four-probe method. The R_s for the sample grown for 10 min was 23.6 kΩ/sq, for 30 min was 1.72 kΩ/sq, and for 60 min was 0.86 kΩ/sq. This value is comparable to typical CVD single-layer graphene [35–38] and lower than reduced graphene oxide [39, 40]. Figure 6a shows the output characteristics (I_D-V_D) of a
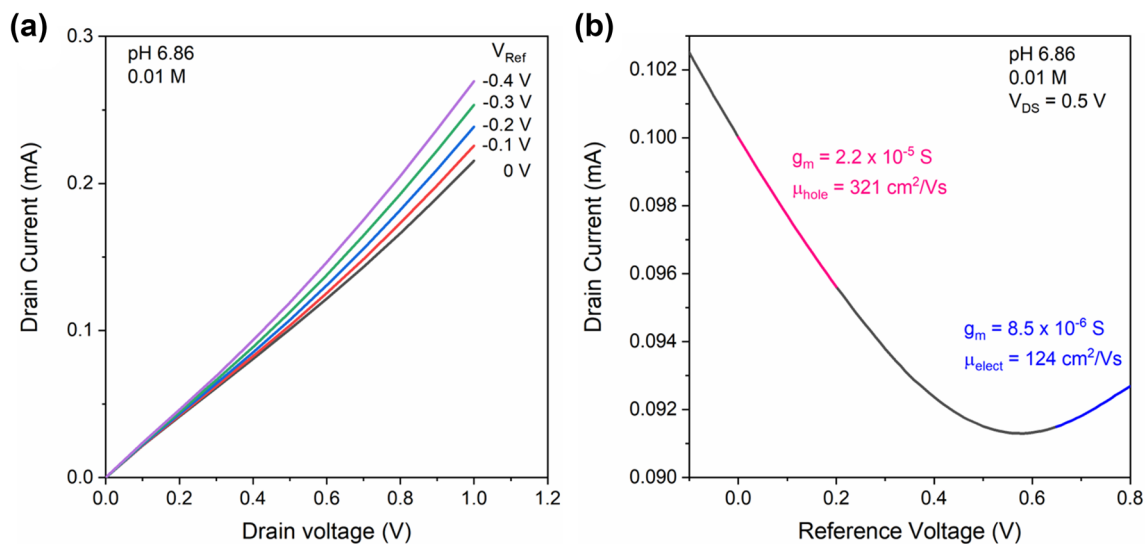

Fig. 6 Measurement results for a typical solution gated GC-FET device with source-drain electrode insulation. **a** I_{DS}–V_{DS} curves for probe gate setup for V_{Ref} values swept from 0 to −0.4 V. **b** Trans-

port characterization of a GC-FET in an electrolyte at pH 6.86 with 0.01 M of NaCl solute

typical solution-gated GC-FETs at five different reference gate voltages (V_{Ref}). The device showed a clear increase in conductance induced by the gate voltage and slightly non-linear behavior, which are typical for Schottky metal/semiconductor junctions. However, the influence of the Schottky barrier and contact resistance at source/drain seemed to be negligible. Figure 6b shows the transfer characteristics of a GC-FET in an electrolyte. When the top gate voltage V_{Ref} swept from -0.1 to 0.8 V, an ambipolar characteristic of the sensor was observed and source-drain current I_{DS} versus V_{Ref} curve showed electron/hole conduction shift at a charge neutral point (CNP) of $V_{Ref} \approx 0.58$ V. The shift in the CNP can be explained by the different scattering cross sections for electrons and may be heavy p-type doping due to a highly disorder graphitic crystallites [41–43]. Therefore, GC can work as either a p-type or an n-type sensor when a small liquid gate voltage is applied to switch its carrier characteristic. Transconductance (g_m) determines how effectively the gate controls the source-drain current and the gm is expressed as;

$$g_m = \Delta I_{DS}/V_{REF} \qquad (1)$$

The g_m was 0 for CNP, and it showed p-type regime (0–0.4 V) and n-type regime (0.7–0.8 V) of the linear region as a highlight in Fig. 6b. The hole and electron mobility were calculated from the linear regime of the transfer characteristics using

$$\mu = g_m \cdot \frac{L}{W} \cdot \frac{1}{CV_D} \qquad (2)$$

where C is the specific capacitance of the dielectric, and μ is the field-effect mobility [44]. The transistor considered in Fig. 6b has an aspect ratio $L/W = 1$, and the gate capacitance is $C(H_2O) = 137$ nF/cm² [44]. The calculated hole and electron mobility were 321 and 124 cm²/Vs at $V_D = 0.5$ V, respectively.

Figure 7 shows a typical pH-dependent transfer characteristics of the GC-FET under different pH values ranging from 4.01 to 12.0. Electrical measurements at a source-drain voltage (V_{DS}) of 0.5 V were used to monitor changes at the channel current at the gate potential was varied as the reference electrode. A positive shift of the CNP, determined as the V_{Ref} value was certainly observed with increasing pH value in the electrolyte. It indicates that a carrier doping occurred when the [H⁺] concentration in the solution changed [45]. The plot of the CNP voltages against pH values indicates that the relationship between pH and conductance is linear over the range from 4.01 to 12.0, and a sensitivity of 20.5 mV/pH was obtained, as showed in the inset of Fig. 7. The results indicate that GC-FETs can be used in pH sensors.

The GC extended gate FET (GC-EGFET) was performed similarly to an operation of a conventional MOSFET with
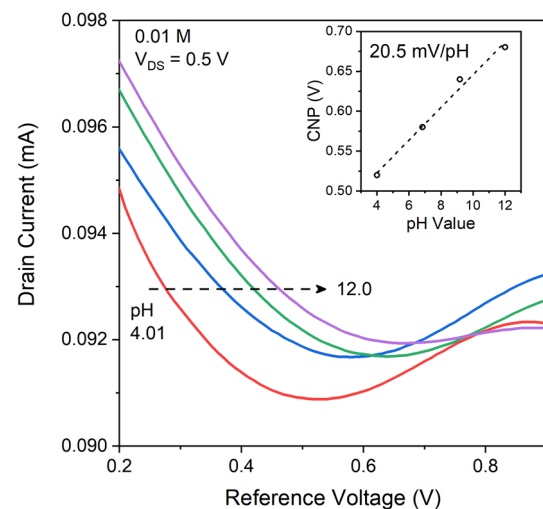

Fig. 7 Source-drain current as a function of the reference potential measured in different pH buffer solutions for a typical GC-FET device. Inset shows top-gate voltage at the charge neutral point (CNP) as a function of pH value. The dashed line is a linear fit to the data points. A sensitivity of 20.5 mV/pH is deduced

the GC sensing membrane utilizing the GC-FET device as a gate electrode. Typical I–V characteristics (I_{DS}–V_{DS}) for the GC pH-EGFET in buffer solutions were recorded in Fig. 8a. The V_{Ref} was held at -0.4 V while the drain to source voltage, the V_{DS} was varied from 0 to 3 V by 0.1 V/step. In the saturation region, the I_{DS} declined steadily as the [H⁺] of buffer solutions decreased from pH 4.01–12.0. The I_{DS} for the saturation region is expressed as

$$I_{DS} = \frac{1}{2} K_n [(V_{Ref} - V_T)^2] \qquad (3)$$

where K_n is the conduction parameter, V_{ref} is the reference electrode voltage [46, 47]. From the equation, the inset of Fig. 8a shows that the GC-EGFET has a linear pH response in the saturation region at $V_{DS} = 2$ V. To obtain the pH sensitivity of the GC-EGFET, the drain to source current-gate reference to source voltage (I_{DS}–V_{Ref}) curves of EGFET were measured in buffer solutions with different pH values as showed in Fig. 8b. The I_{DS}–V_{Ref} curves shifted to a positive voltage while the samples were immersed into higher pH value of buffer solutions in a concentration range between pH 4.01 and 12.0. The result shows the GC-EGFET has a linear pH sensitivity of 27.8 mV/pH.

Three sets of devices were fabricated to evaluate the reproducibility of GC pH sensors. Table 1 shows the sensitivity results of the reproducibility test of three independently developed GC FET/pH sensor electrodes in different buffer solutions at pH 4 to pH 12. The relative standard deviation (RSD) determined from these measurements for GC-FET was 5.5% and for GC-EGFET was 6.5%, respectively, confirming that both GC-FET and

GC-EGFET have good reproducibility. GC-EGFET sensors tended to detect higher sensitivity than that of GC-FET configuration. In Table 2, we compare the pH sensitivity of our GC sensor with other CNTs, graphene, and rGO FET pH sensors reported in the literature. It is worth noticing that this sensitivity of the GC pH sensors is similar

to the one reported for SWCNT (20 mV/pH) [48], for mechanically exfoliated graphene (19 mV/pH) [50], and for CVD graphene (26 mV/pH) [52]. Indeed, preceding studies show a large variation ranging from 6 to 99.8 mV/pH using sp^2-carbon materials obtained from different methods. The sensing mechanism remains unclear yet,
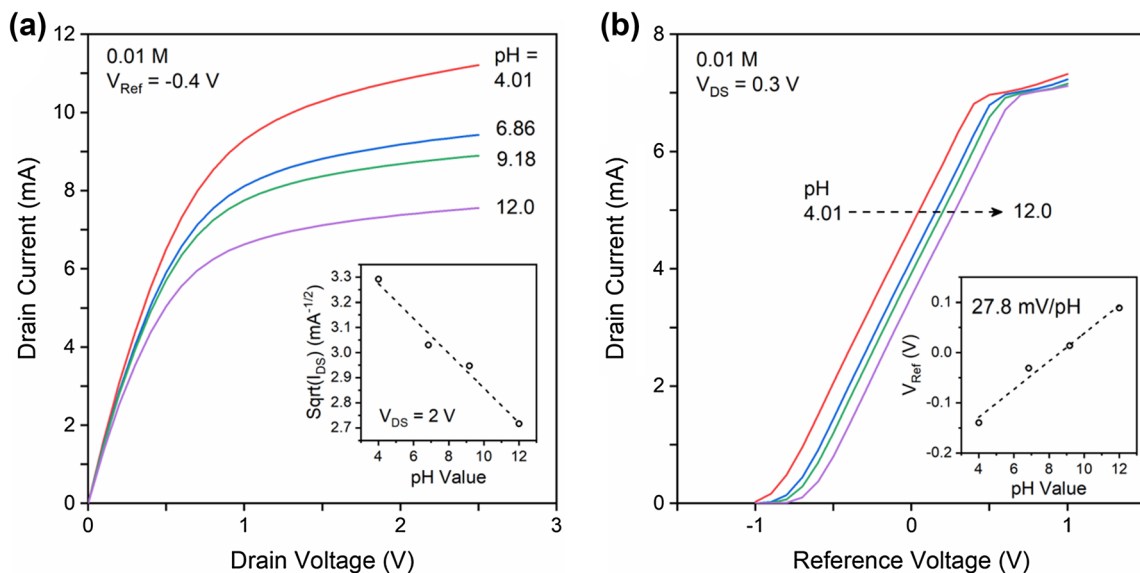

Fig. 8 Measurement results for a typical extended gated GC-FET device with GC electrode. **a** I_{DS}–V_{DS} curves for probe gate setup for V_{Ref} values for varying pH values. Inset shows pH sensitivity of square root of I_{DS} for measurements between pH 4.01 and 12.0. **b** Transport characterization of a GC-FET in an electrolyte at pH 6.86 with 0.01 M of NaCl solute. Inset shows reference electrode voltage measured under constant voltage constant current and exposed to various pH values

Table 1 The average pH sensitivity of the combination of the devices

Device name	Configuration	Sensitivity (mV/pH)				
		Device 1	Device 2	Device 3	Average	RSD (%)
GC-FET	Solution gated FET	20.5	22.8	21.2	21.5	5.5
GC-EGFET	Extended gate FET	27.8	27.1	24.5	26.5	6.5

Table 2 Comparison of pH performance for different sp^2 carbon materials

Materials	Configuration	Sensitivity (mV/pH)	pH range	References
GC	Solution-gate	21.5	4.0–12.0	This work
GC	Extended-gate	26.5	4.0–12.0	This work
SWCNT	Solution-gate	20	4.0–9.0	[48]
MWCNT	Extended-gate	16.2–36.4	2.0–12.0	[55]
EP graphene	Solution-gate	98.8	2.0–12.0	[49]
EP graphene	Solution-gate	19	3.0–12.0	[50]
ME graphene	Solution-gate	27.8	4.0–8.2	[45]
ME graphene	Solution-gate	17	6.0–9.0	[42]
CVD graphene	Solution-gate	6	5.0–10.0	[51]
CVD graphene	Solution-gate	21	4.3–8.4	[52]
CVD graphene	Solution-gate	16.6	4.0–10.0	[54]
rGO	Solution-gate	29.2	6.0–9.0	[53]

EP epitaxial, *ME* mechanical exfoliated

however, the GC films can be adapted to comparable for the pH sensing membrane.

4 Conclusions

We have successfully synthesized thin film of glassy carbon by chemical vapor deposition using ethanol as a carbon source. A thermal pyrolysis process of ethanol provides high quality GC film with graphite like structure of a turbostratic layer stacking. The growth time dependence clarifies the film growth has a three-dimensional nature. The domain size of nano-graphitic crystallite was about 13 nm, which was not changed with the growth time. XPS analysis showed that the deposited films have carbon atoms consisting of an almost sp^2 binding structure. We investigated solution gated GC-FET and GC-EGFET for pH sensor applications. The GC-FET showed good gate transfer characteristics in electrolytes. A high mobility of holes for 321 cm^2/Vs and electrons for 124 cm^2/Vs were obtained. The average pH sensitivity of GC-FET and GC-EGFET is 21.5 mV/pH and 26.5 mV/pH, respectively, which are comparable for graphene-based solution gating pH sensors. These results indicate GC based FETs are promising candidates for the development of biological sensors.

Compliance with ethical standards

References

1. Kawamura K, Jenkins GM (1970) A new glassy carbon fibre. J Mater Sci 5:262–267
2. Harris PJF (2004) Fullerene-related structure of commercial glassy carbons. Philos Mag 84:3159–3167
3. Harris PJF (2013) Fullerene-like models for microporous carbon. J Mater Sci 48:565–577
4. Jurkiewicz K, Pawlyta M, Zygadło D et al (2018) Evolution of glassy carbon under heat treatment: correlation structure–mechanical properties. J Mater Sci 53:3509–3523
5. Parker S, Imberti S, Callear S, Albers P (2013) Structural and spectroscopic studies of a commercial glassy carbon. Chem Phys 427:44–48
6. Guan W, Duan X, Reed M (2014) Highly specific and sensitive non-enzymatic determination of uric acid in serum and urine by extended gate field effect transistor sensors. Biosens Bioelectron 51:225–231
7. Hoshikawa Y, Castro-Muñiz A, Komiyama H et al (2014) Remarkable enhancement of pyrolytic carbon deposition on ordered mesoporous silicas by their trimethylsilylation. Carbon 67:156–167
8. Enterría E, Figueiredo JL (2016) Nanostructured mesoporous carbons: tuning texture and surface chemistry. Carbon 108:79–102
9. Yi Y, Weinberg G, Prenzel M et al (2017) Electrochemical corrosion of a glassy carbon electrode. Catal Today 295:32–40
10. Thiha A, Ibrahim F, Muniandy S et al (2018) All-carbon suspended nanowire sensors as a rapid highly-sensitive label-free chemiresistive biosensing platform. Biosens Bioelectron 107:145–152
11. Libbrecht W, Verberckmoes A, Thybaut J et al (2017) Soft templated mesoporous carbons: tuning the porosity for the adsorption of large organic pollutants. Carbon 116:528–546
12. Hassan YM, Caviglia Hemanth et al (2017) High temperature SU-8 pyrolysis for fabrication of carbon electrodes. J Anal Appl Pyrolsis 125:91–99
13. Zhao Q-L, Bao L, Luo Q-Y et al (2009) Surface manipulation for improving the sensitivity and selectivity of glassy carbon electrodes by electrochemical treatment. Biosens Bioelectron 24:3003–3007
14. Hassine CBA, Barhoumi H (2018) Electrochemical study of a glassy carbon electrode modified by poly-4-nitroaniline murexide and its sensitivity for metal ions. Anal Biochem 560:30–38
15. Hsia B, Kim M, Vincent M et al (2013) Photoresist-derived porous carbon for on-chip micro-supercapacitors. Carbon 57:395–400
16. Ferrer-Argemi L, Aliabadi E, Cisquella-Serra A et al (2018) Size-dependent electrical and thermal conductivities of electro-mechanically-spun glassy carbon wires. Carbon 130:87–93
17. Natu R, Islam M, Gilmore J, Martinez-Duarte R (2018) Shrinkage of SU-8 microstructures during carbonization. J Anal Appl Pyrolsis 131:17–27
18. Mohamed H (2016) Screen-printed disposable electrodes: pharmaceutical applications and recent developments. TrAC Trends Anal Chem 82:1–11
19. Chu Z, Peng J, Jin W (2017) Advanced nanomaterial inks for screen-printed chemical sensors. Sens Actuators B Chem 243:919–926
20. Meyer JC, Geim AK, Katsnelson MI et al (2007) The structure of suspended graphene sheets. Nature 446:60–63
21. Li X, Cai W, An J et al (2009) Large-area synthesis of high-quality and uniform graphene films on copper foils. Science 324:1312–1314
22. Shah K, Tali B (2016) Synthesis of carbon nanotubes by catalytic chemical vapour deposition: a review on carbon sources, catalysts and substrates. Mater Sci Semicond Process 41:67–82
23. Hou P-X, Liu C, Cheng H-M (2008) Purification of carbon nanotubes. Carbon 46:2003–2025
24. Edwards ER, Antunes EF, Botelho EC et al (2011) Evaluation of residual iron in carbon nanotubes purified by acid treatments. App Surf Sci 258:641–648
25. Janas D, Rdest M, Koziol K (2017) Free-standing films from chirality-controlled carbon nanotubes. Mater Des 121:119–125

26. Harris PJF, Burian A, Duber S (2000) High-resolution electron microscopy of a microporous carbon. Philos Mag Lett 80(6):381–386

27. Sze S-K, Siddique Sloan JJ, Escribano R (2001) Raman spectroscopic characterization of carbonaceous aerosols. Atmos Environ 35:561–568

28. Zickler G, Smarsly B, Gierlinger N et al (2006) A reconsideration of the relationship between the crystallite size La of carbons determined by X-ray diffraction and Raman spectroscopy. Carbon 44:3239–3246

29. Larouche N, Stansfield B (2010) Classifying nanostructured carbons using graphitic indices derived from Raman spectra. Carbon 48:620–629

30. Lentz CM, Samuel BA, Foley HC, Haque MA (2011) Synthesis and characterization of glassy carbon nanowires. J Nanomater 2011:1–8

31. Pawlyta M, Rouzaud J-N, Duber S (2015) Raman microspectroscopy characterization of carbon blacks: spectral analysis and structural information. Carbon 84:479–490

32. Ferrari A (2007) Raman spectroscopy of graphene and graphite: disorder, electron–phonon coupling, doping and nonadiabatic effects. Solid State Commun 143:47–57

33. Eckmann A, Felten A, Mishchenko A et al (2012) Probing the nature of defects in graphene by Raman spectroscopy. Nano Lett 12:3925–3930

34. Webb M, Palmgren P, Pal P et al (2011) A simple method to produce almost perfect graphene on highly oriented pyrolytic graphite. Carbon 49:3242–3249

35. Li X, Zhu Y, Cai W et al (2009) Transfer of large-area graphene films for high-performance transparent conductive electrodes. Nano Lett 9:4359–4363

36. Lee M-S, Lee K, Kim S-Y et al (2013) High-performance, transparent, and stretchable electrodes using graphene-metal nanowire hybrid structures. Nano Lett 13:2814–2821

37. Maarouf A, Kasry A, Chandra B, Martyna G (2016) A graphene–carbon nanotube hybrid material for photovoltaic applications. Carbon 102:74–80

38. Wu X, Asselberghs I, Politou M et al (2017) Doping of graphene for the application in nano-interconnect. Microelectron Eng 167:42–46

39. Wassei J, Kaner R (2010) Graphene, a promising transparent conductor. Mater Today 13:52–59

40. Qiao Z, Qin C, Gao Y et al (2015) Modulation of the optical transmittance in monolayer graphene oxide by using external electric field. Sci Rep 5:14441-1–14441-9

41. Jang C, Adam S, Chen J-H et al (2008) Tuning the effective fine structure constant in graphene: opposing effects of dielectric screening on short- and long-range potential scattering. Phys Rev Lett 101:146805-1–146805-4

42. Cheng Z, Li Q, Li Z et al (2010) Suspended graphene sensors with improved signal and reduced noise. Nano Lett 10:1864–1868

43. Li P, Liu B, Zhang D et al (2016) Graphene field-effect transistors with tunable sensitivity for high performance Hg(II) sensing. Appl Phys Lett 109:153101-1–153101-5

44. Huang Y, Sutter E, Wu L et al (2018) Thick layered semiconductor devices with water top-gates: high on-off ratio field-effect transistors and aqueous sensors. ACS Appl Mater Interfaces 10:23198–23207

45. Ohno Y, Maehashi K, Yamashiro Y, Matsumoto K (2009) Electrolyte-gated graphene field-effect transistors for detecting pH and protein adsorption. Nano Lett 9:3318–3322

46. Batista PD, Mulato M, Graeff CFO, Fernandez FJR, Marques FC (2006) SnO_2 extended gate field-effect transistor as pH sensor. Braz J Phys 36:478–481

47. Yao P-C, Chiang J-L, Lee M-C (2014) Application of sol-gel TiO_2 film for an extended-gate H+ ion-sensitive field-effect transistor. Solid State Sci 28:47–54

48. Back JH, Shim M (2006) pH-dependent electron-transport properties of carbon nanotubes. J Phys Chem B 110:23736–23741

49. Ang P, Chen W, Wee A, Loh K (2008) Solution-gated epitaxial graphene as pH sensor. J Am Chem Soc 130:14392–14393

50. Ristein J, Zhang W, Speck F et al (2010) Characteristics of solution gated field effect transistors on the basis of epitaxial graphene on silicon carbide. J Phys D Appl Phys 43:345303

51. Fu W, Nef C, Knopfmacher O et al (2011) Graphene transistors are insensitive to pH changes in solution. Nano Lett 11:3597–3600

52. Mailly-Giacchetti B, Hsu A, Wang H et al (2013) pH sensing properties of graphene solution-gated field-effect transistors. J Appl Phys 114:084505

53. Sohn I-Y, Kim D-J, Jung J-H et al (2013) pH sensing characteristics and biosensing application of solution-gated reduced graphene oxide field-effect transistors. Biosens Bioelectron 45:70–76

54. Wang YY, Burke PJ (2013) A large-area and contamination-free graphene transistor for liquid-gated sensing applications. Appl Phys Lett 103:052103

55. Hung S-C, Cheng N-J, Yang C-F, Lo Y-P (2014) Investigation of extended-gate field-effect transistor pH sensors based on different-temperature-annealed bi-layer MWCNTs-In2O3 films. Nanoscale Res Lett 9:502